Decadal Variability in ENSO Predictability and Prediction

BEN P. KIRTMAN

Center for Ocean–Land–Atmosphere Studies, Institute of Global Environment and Society, Calverton, Maryland

PAUL S. SCHOPF

George Mason University, Fairfax, Virginia, and
Center for Ocean–Land–Atmosphere Studies, Institute of Global Environment and Society, Calverton, Maryland

(Manuscript received 19 May 1997, in final form 7 January 1998)

ABSTRACT

A simple coupled model is used to examine decadal variations in El Niño–Southern Oscillation (ENSO) prediction skill and predictability. Without any external forcing, the coupled model produces regular ENSO-like variability with a 5-yr period. Superimposed on the 5-yr oscillation is a relatively weak decadal amplitude modulation with a 20-yr period. External uncoupled atmospheric ''weather noise'' that is determined from observations is introduced into the coupled model. Including the weather noise leads to irregularity in the ENSO events, shifts the dominant period to 4 yr, and amplifies the decadal signal. The decadal signal results without any external prescribed changes to the mean climate of the model.

Using the coupled simulation with weather noise as initial conditions and for verification, a large ensemble of prediction experiments were made. The forecast skill and predictability were examined and shown to have a strong decadal dependence. During decades when the amplitude of the interannual variability is large, the forecast skill is relatively high and the limit of predictability is relatively long. Conversely, during decades when the amplitude of the interannual variability is low, the forecast skill is relatively low and the limit of predictability is relatively short. During decades when the predictability is high, the delayed oscillator mechanism drives the sea surface temperature anomaly (SSTA), and during decades when the predictability is low, the atmospheric noise strongly influences the SSTA. Additional experiments indicate that the relative effectiveness of the delayed oscillator mechanism versus the external noise forcing in determining interannual SSTA variability is strongly influenced by much slower timescale (decadal) variations in the state of the coupled model.

1. Introduction

As a result of the Tropical Ocean Global Atmosphere program, experimental and operational El Niño–Southern Oscillation (ENSO) predictions are regularly made that have demonstrated a degree of accuracy in forecasting tropical Pacific sea surface temperature anomalies (SSTA) under certain circumstances [e.g., Zebiak and Cane (1987); Barnett et al. (1993); Kleeman (1993); Ji et al. (1994); Chen et al. (1995); Ji et al. (1996); Kirtman et al. (1997); Kirtman and Zebiak (1997); see Latif et al. (1998) for a review of ENSO prediction studies]. However, the wide variety of techniques being used for prediction [e.g., the National Oceanic and Atmospheric Administration Experimental Long Lead Forecast Bulletin], the seasonality in forecast skill (e.g., Zebiak and Cane 1987), and the decadal variations in forecast skill (e.g., Balmaseda et al. 1995) are evidence of the fact that, despite our current level of understanding, much is to be learned concerning the limits of ENSO predictability.

While many of the ENSO prediction systems referenced above are substantially different in their formulation and sophistication, they uniformly have low forecast skill in the 1990s compared to previous decades. For example, Ji et al. (1996) found, using a state-of-the-art coupled general circulation model, that the ENSO forecast skill during 1982–92 was considerably higher than during 1990–95. Similarly, even with an improved initialization strategy (Chen et al. 1995), the Zebiak and Cane (1987) model has lower skill during the 1990s. Similar decadal variability in forecast skill has also been detected in the Kirtman et al. (1997) prediction system and by Balmaseda et al. (1995) in their hybrid coupled model.

The contrast in prediction skill between the 1980s and the early 1990s is quite clear. What remains unclear is whether this contrast was a statistical fluke or whether there was some fundamental change in the coupled ENSO system. The results presented here indicate that

Corresponding author address: Dr. Ben P. Kirtman, Center for Ocean–Land–Atmosphere Studies, Institute of Global Environment and Society, 4041 Powdermill Road, Suite 302, Calverton, MD 20705-3106.
E-mail: kirtman@cola.iges.org

relatively slow timescale changes in the coupled system are responsible for this contrast in prediction skill. Understanding the mechanims for the contrast in prediction skill allows for considerable optimism in terms of ENSO prediction. Given this understanding, it may be possible to a priori predict whether the coupled system is in a relatively predictable or unpredictable regime.

There is considerable mounting observational evidence that decadal variations of ENSO are part of the natural variability of the tropical Pacific. For example, Wang (1995) found interdecadal changes in the mean background state between the warm events prior to the late 1970s and after the late 1970s. In 1977, the tropical Pacific experienced an abrupt warming, which, in turn, affected the onset of the warms events. Before 1977, the warming along the South American coast led the warming in the central Pacific, whereas after 1977 the warm events first appeared in the central Pacific. Zhang et al. (1997) also found similar decadal variations in SST during the period 1903–93. Torrence and Webster (1996) applied a 15-yr running variance to SSTA data, and found that the frequency and amplitude of ENSO events change on interdecadal timescales, with low variability during midcentury and high variance at the beginning and the end of the twentieth century. Persistence SSTA forecasts were also found to be more skillful during decades when the variance was relatively large.

The mechanism for these decadal variations in ENSO variability is not well understood. Trenberth and Hoar (1997) have suggested that the prevailing warm conditions during the 1990s is unique when compared with the remainder of the historical record, and is a result of anthropogenic global warming. Gu and Philander (1997), on the other hand, argue that these decadal variations are part of the natural variability and should be expected. Gu and Philander (1997) suggest a mechanism by which the tropical and extratropical oceans interact to produce decadal variations in the mean thermocline structure of the tropical Pacific.

The Gu and Philander (1997) mechanism works as follows. Suppose the tropical Pacific is relatively warm. The extratropical atmospheric response to this warming is an increase in the surface westerlies. The increased westerlies cool the surface of the extratropical ocean through an increased latent heat flux. The relatively cool extratropical surface water is subducted and arrives in the tropical thermocline approximately 12 years later, reversing the warming and initiating a relatively cool period. As the Tropics cool, the extratropical westerlies weaken, warming the surface water and ultimately producing a relatively warm tropical thermocline approximately 12 years later. This mechanism results in a repeating decadal cycle where the period is determined by the time it takes the subducted extratropical water to arrive in the tropical thermocline. It is not known how this mechanism would affect ENSO prediction and predictability.

Understanding how decadal variations in the tropical Pacific affect ENSO prediction and predictability is complicated by the fact that there is no clear understanding of the mechanisms that lead to its irregularity and ultimately the loss of predictability. While the basic mechanism that drives ENSO, the so-called delayed oscillator (Suarez and Schopf 1988; Battisti and Hirst 1989), is well established, current thinking suggests two possibilities for the irregularity of ENSO: 1) deterministic chaos within the nonlinear dynamics of the coupled system (Munnich et al. 1991; Jin et al. 1994; Tziperman et al. 1994; Chang et al. 1994; Chang et al. 1995), and 2) uncoupled atmospheric ''noise'' on monthly or seasonal mean timescales (Battisti 1989; Kleeman and Power 1994; Blanke et al. 1997; Eckert and Latif 1997; Kleeman and Moore 1997).

With respect to the first mechanism, Tziperman et al. (1994) and Jin et al. (1994) argue that nonlinear interactions between the ENSO mode and the annual cycle leads to chaotic interannual variability. Both these studies noted a transition by the quasi-periodicity route to chaos that is often found in periodically forced nonlinear systems. With the Jin et al. (1994) model, the parameter space corresponding to periodic regimes is considerably larger than chaotic regimes (see Fig. 6, Jin et al. 1996). Neelin et al. (1998) point out that this suggests that there is a greater likelihood that the irregularity of ENSO is due external uncoupled atmospheric noise as opposed to internal nonlinear dynamics.

Kleeman and Power (1994) used observed wind stress data to incorporate noise into their coupled model and found that it strongly limits the prediction skill. Eckert and Latif (1997) used similar techniques in a more sophisticated coupled model. Blanke et al. (1997) applied a different technique to isolate the noise forcing. They used their empirical atmospheric component model forced with observed SSTA to define a wind stress anomaly that is linearly related to the SSTA. By subtracting this wind stress anomaly from the observed wind stress anomaly they obtain an estimate for the noise component of the wind stress forcing.

In this paper we examine how atmospheric noise alone in a simple coupled model without deterministic chaotic behavior can lead to decadal variability in ENSO predictability and prediction skill. The focus of the predictability and prediction experiments presented here is to demonstrate how uncoupled atmospheric noise can lead to decadal variations in the character of ENSO. The coupled model used in the simulation and predictability experiments here is described in detail by Kirtman (1997). The model consists of a statistical atmosphere coupled to the Zebiak and Cane (1986) ocean model, and, in an extended integration without uncoupled atmospheric noise, the model produces a regular 5-yr oscillation. On the other hand, when uncoupled atmospheric noise is included in the simulation, the spectral density becomes red and the dominant oscillation period shifts to approximately 48 months much like the observed spectral density. The simulation with atmospher-

ic noise produces decades where the interannual variability is strong and regular and decades where the variability is weak and highly irregular.

A series of idealized prediction and predictability experiments indicate that the forecast skill has a strong decadal dependence without any prescribed changes in the mean climate. We have not externally modified the mean state of the coupled model to produce this decadal dependence. In some decades, the NINO3 (SSTA averaged over 5°S–5°N, 150°–90°W) correlation coefficient remains above 0.6 for lead times of up to 15 months, whereas in other decades the correlation drops below 0.6 after only 5 months. It is not surprising that during decades when the interannual variability is regular the predictability is high and during decades when the interannual variability is irregular the predictability is low. Prediction experiments using the delayed oscillator equation directly indicate that, during the predictable decades, the SSTA variability can be described as being in the delayed oscillator regime. Conversely, during the unpredictable decades, the delayed oscillator mechanism does not dominate and the SSTA variability is driven by the noise.

A series of coupled model experiments demonstrate that the relatively slow timescale (decadal) variability in the mean state of the coupled model determines whether the delayed oscillator mechanism or the noise forcing dominates the interannual SSTA variability. For example, during the predictable decades, the decadal mean anomaly is characterized by westerly wind stress anomalies and warm SSTA. When this mean state is prescribed in the coupled model without noise, regular ENSO oscillations that are consistent with delayed oscillator physics are maintained. The unpredictable decades, however, are characterized by mean easterly wind stress anomalies and cold SSTA. Once this later mean state is prescribed in the coupled model without noise, there are no ENSO oscillations implying that, when noise is included, the SSTA is more susceptible to being driven by the noise forcing. This result is confirmed by repeating these prescribed mean simulations with uncoupled noise forcing.

The remainder of the paper is outlined as follows. Section 2 describes the model and the response to the external uncoupled noise forcing. The predictability and prediction experiments are described in section 3, and section 4 presents results from coupled model simulations that isolate the effects of decadal variations of the mean and the uncoupled noise forcing. Finally, section 5 has the concluding remarks.

2. The coupled model

In these experiments, we use a coupled ocean–atmosphere model that consists of a very simple statistical atmosphere coupled to the ocean model used in the Zebiak and Cane (1987) coupled model hereinafter called the Z–C model. The dynamics of the ocean model are described by linear reduced gravity equations of motion that simulate thermocline depth anomalies and depth-averaged baroclinic currents. A shallow frictional layer of constant depth (50 m) is added to the top of the model to simulate the surface intensification of wind-driven currents. The equation governing the SST includes the effects of horizontal and vertical advection of temperature by both mean and anomalous currents. The annual cycle is included in the model by prescribed mean current, mean temperature, and mean upwelling. The SST equation also includes an anomalous surface heat flux that acts to damp the SSTA to zero. An annual mean thermocline depth that is only a function of longitude is prescribed.

The atmospheric component is modeled as follows:

$$\tau_x = \alpha(x, y)\text{NINO3}, \quad \tau_y = \beta(x, y)\text{NINO3},$$

where NINO3 is the SSTA in the coupled model averaged over the so-called NINO3 region (5°S–5°N, 150°–90°W), and τ_x and τ_y are the zonal and meridional wind stress anomaly, respectively. The structure functions α and β were determined by linearly regression of the observed time series of NINO3 SSTA from 1964–94 onto the Florida State University (FSU) analyzed pseudostress (Goldenberg and O'Brien 1981). The FSU wind stress data was also detrended. As with the Zebiak and Cane (1987) ocean model, the FSU pseudostress is converted into a wind stress by assuming a constant drag coefficient of 2×10^{-2} and a constant air density of 1 kg m^{-3}. The behavior of this coupled model in extended integrations is documented in Kirtman (1997) and produces regular ENSO oscillations with a well-defined spectral peak at 5 yr.

Response to uncoupled atmospheric noise

As mentioned in the introduction, there is substantial debate concerning the mechanisms that lead to the irregularity of ENSO. Part of the reason for the debate is that many of the simple models used for ENSO simulation and prediction, such as the coupled model presented here, do not exhibit irregular behavior (e.g. Battisti 1988; Kleeman 1993). In order to produce irregular behavior, ''atmospheric noise'' with a monthly timescale is added to the atmospheric component of the coupled system (e.g., Battisti 1989; Kleeman and Power 1994).

It should be noted, however, that the Z–C model simulates irregular ENSO behavior without imposing atmospheric noise. Moreover, Zebiak (1989) found that incorporating atmospheric noise did little to change the coupled model behavior. Mantua and Battisti (1995) have shown that the reason for this difference between these fairly similar coupled models is due to a relatively fast timescale westward propagating coupled instability in the Zebiak and Cane (1987) coupled model. Mantua and Battisti (1995) argued that this so-called mobile mode is not detected in the observational record. The reason the Z–C model is relatively insensitive to the

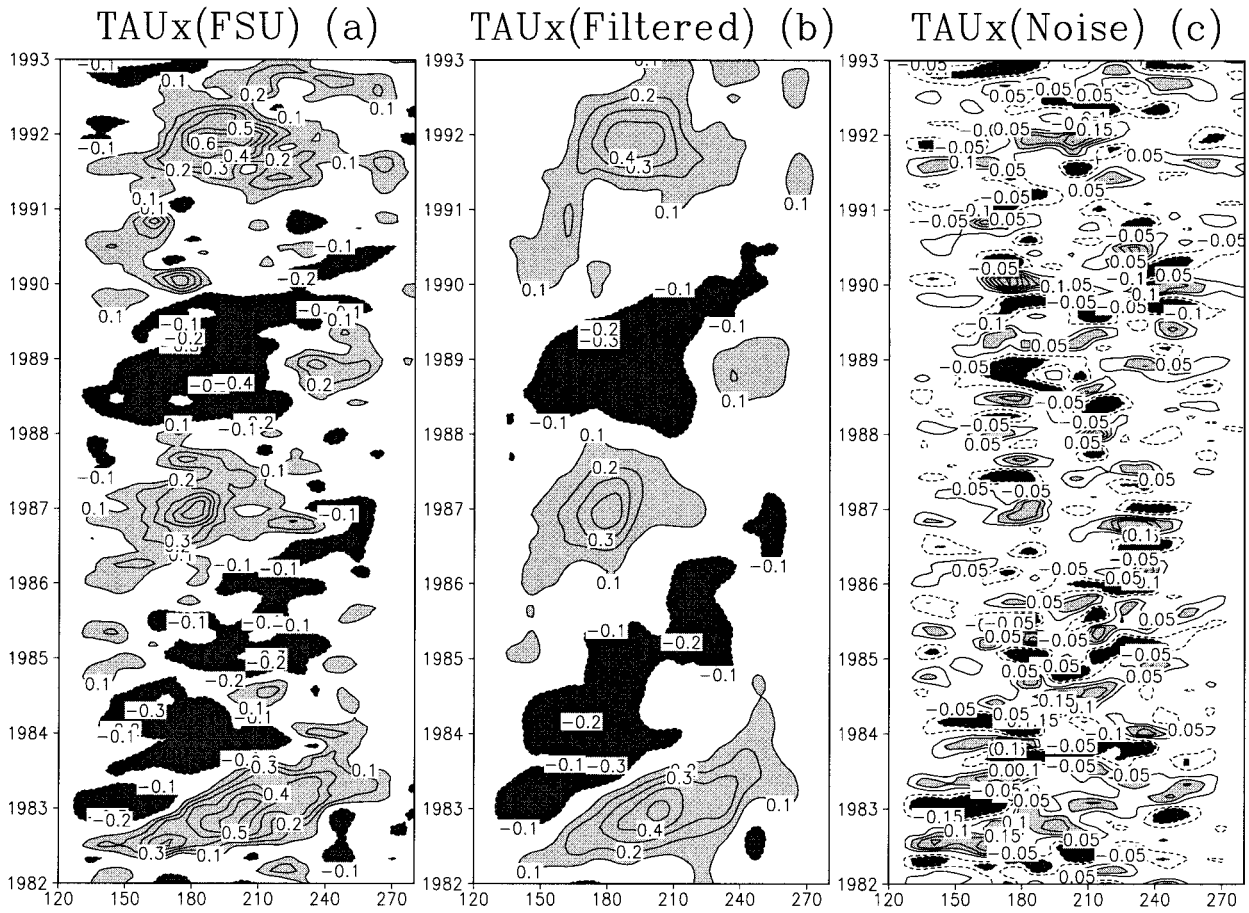

FIG. 1. Time–longitude cross section along the equator of the (a) observed FSU zonal wind stress, (b) the FSU zonal wind stress with a 9-month running mean applied, and (c) the difference between the FSU zonal wind stress with and without the running mean. In (a) and (b) the contour interval is 0.1 dyn cm^{-1} and in (c) the contour interval is 0.05 dyn cm^{-1}.

noise forcing is that it already exhibits irregular behavior. The additional noise does not significantly alter the character of the irregularity.

In order to introduce irregular ENSO variability in the experiments presented here, we have taken an approach similar to Kleeman and Power (1994). The motivation for this approach is that we want to incorporate atmospheric noise that has the observed spatial and temporal statistics. The observed monthly mean wind stress is filtered so that only the high-frequency component remains. A 9-month running mean is applied to the FSU wind stress from 1964–94. The running mean is then subtracted from the data leaving what will be referred to as atmospheric noise. Figures 1a–c show the unfiltered FSU zonal wind stress, the zonal wind stress after the 9-month running mean has been applied, and the remaining atmospheric noise, respectively. The time series along the equator is plotted for the period of 1982–92. The ENSO signal dominates both the filtered (Fig. 1b) and unfiltered (Fig. 1a) zonal wind stress. The noise (Fig. 1c) has spatial and temporal scales that are considerably shorter than the ENSO signal, but are distinctly not random and occur on temporal scales that are longer than typical atmospheric synoptic variability. The noise is dominated by a 30–90-day timescale. A spectral analysis of the noise indicates very little power on timescales longer than 90 days.

There are other ways of specifying the noise component (i.e., Blanke et al. 1997) so that it is white in time and or space. While the procedure presented here for separating the noise from the ENSO signal is somewhat ad hoc, we believe it retains the temporal and spatial statistics of the noise that is important in terms of limiting ENSO predictability.

The noise is incorporated into the coupled model to preserve as much of the temporal and spatial statistics as simply as possible. At the initial time, a random date is chosen to begin sampling the noise dataset. Each successive simulation month samples each successive noise month. Eventually, the simulation reaches the end of the noise dataset and a new start month is randomly selected. Although it is not shown here, it turns out that

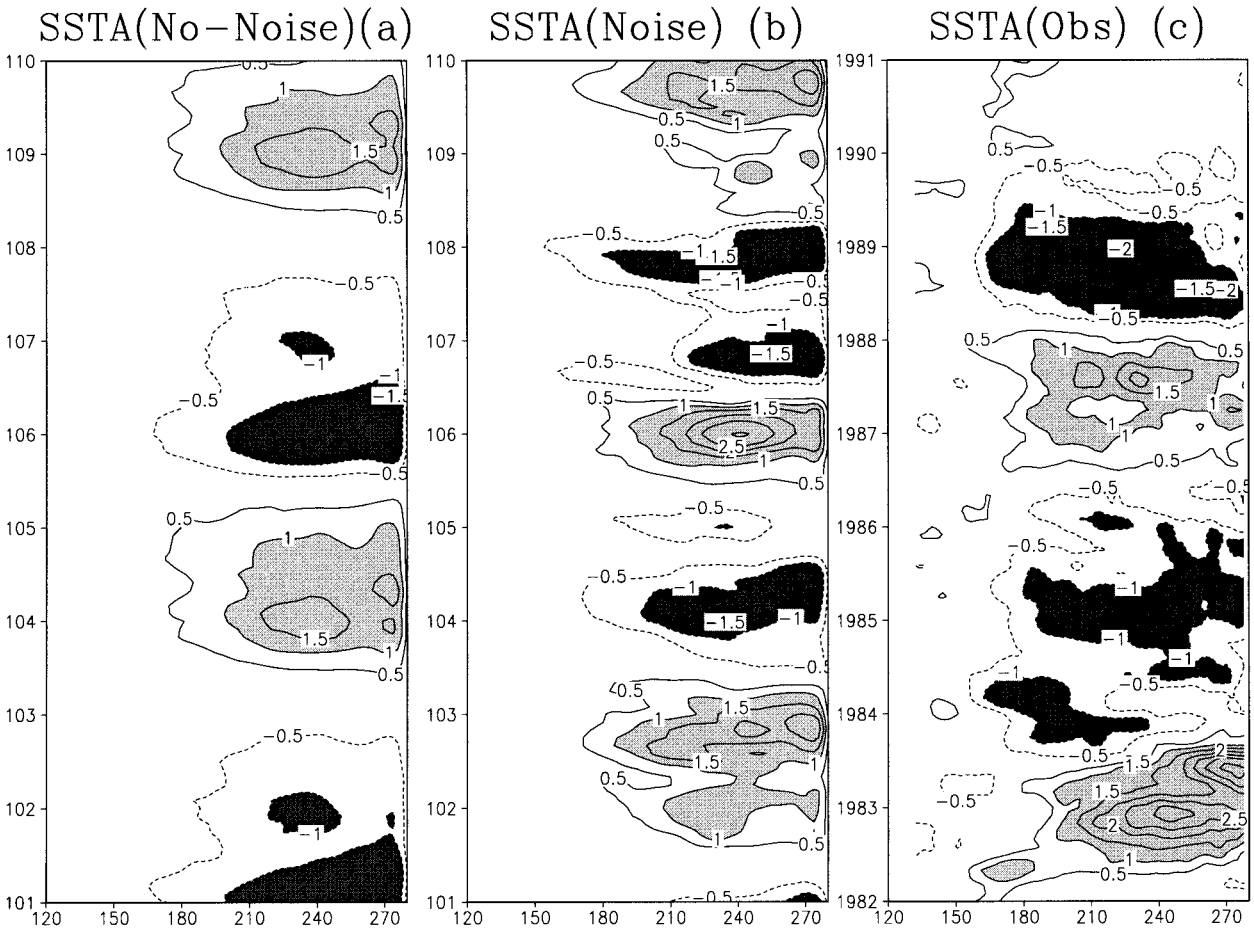

FIG. 2. Time–longitude cross section along the equator of the SSTA from the (a) coupled-model simulation without noise, (b) the coupled model with uncoupled noise forcing, and (c) the observations from 1982–90. The contour interval in all three panels is 1.0°C.

the temporal coherence of the noise affects the forecast skill of the prediction experiments described in the next section. When the temporal coherence of the noise is removed the prediction skill improves. The more temporally and spatially coherent the noise is, the more effective it is at limiting the predictability of the model.

The initial conditions for the control simulation are taken from an extended integration of the ocean model forced with observed FSU wind stress. Simulations both with and without the noise forcing are made. Each simulation is integrated for at least 200 yr and results are shown after the first 100 yr have been discarded.

Figures 2a–c show time–longitude cross sections of the simulated SSTA with and without atmospheric noise and the observed SSTA, respectively. For the model results, simulation years 101–110 are plotted and for the observed 1982–91 is plotted. In the same format as Figs. 2a–c, Figs. 3a–c show the simulated and observed zonal wind stress anomaly. For example, the simulation without noise (Figs. 2a and 3a) captures some of the basic features of the observed ENSO characteristics. The SSTA is strongest in the eastern Pacific with little or no anomaly to the west of the date line. The ENSO events reach their peak amplitude during the boreal winter season much like the observed signal, and there is some asymmetry between cold and warm events. However, without noise, the oscillation period is too long compared to the observations and the duration of the warm and cold events is also too long. Details of the simulation without noise and what determines the oscillation period are discussed in Kirtman (1997).

Adding uncoupled atmospheric noise to the model (Figs. 2b and 3b) alters several characteristics of the extended simulation. Foremost, the ENSO events occur at irregular intervals and the duration of the warm and cold periods are in better agreement with the observed interannual variability. Perhaps it is not surprising that the simulated zonal wind stress with noise is qualitatively similar to the observed.

In the frequency domain there is also an important difference between the simulations with and without noise. Using the last 100 yr of the coupled model simulation with uncoupled atmospheric noise and 45 yr of observed SSTA (1950–94), the spectral density of the

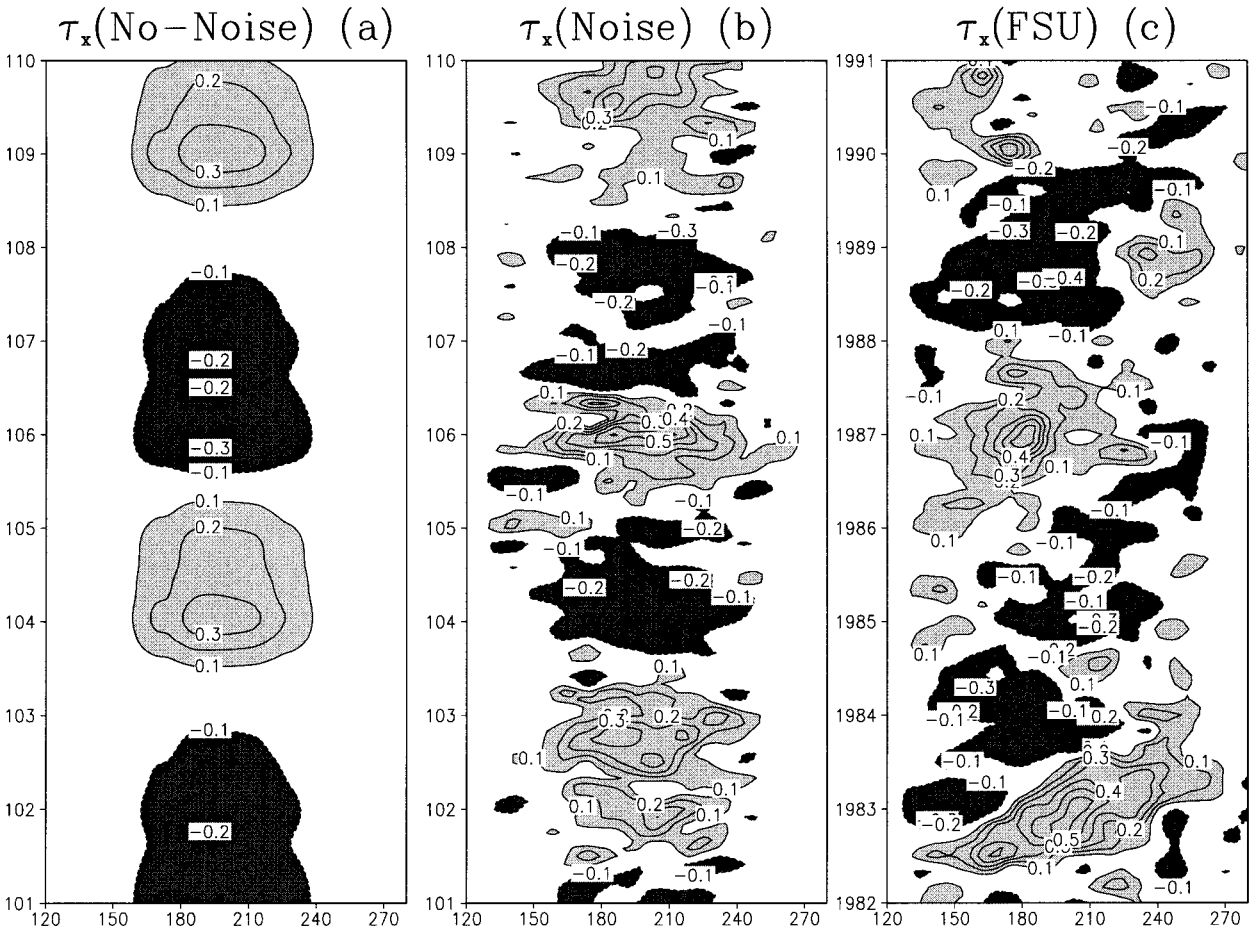

FIG. 3. Time–longitude cross section along the equator of the zonal wind stress anomaly from the (a) coupled model with out noise, the (b) coupled model with uncoupled noise forcing, and the (c) FSU observations from 1982–90. The contour interval in all three panels in 0.1 dyn cm^{-1}.

NINO3 SSTA is plotted in Figs. 4a,b. The spectral density calculation (for both the time series and the red noise fit) is based on the Fourier method. For additional details, the reader is referred to Jenkins and Watts (1968). The spectral density for the simulation without noise is not shown, but has a very narrow peak at 60 months. The dominant observed period (Fig. 4a) is about 48 months, although the spectral density is greater than red noise for periods between 36 and 63 months. The simulated spectral density has a somewhat narrower peak with larger amplitude at 48 months. Remarkably, the atmospheric noise causes the dominant period to shift from 5 yr to about 4 yr. At low frequencies, the observed spectral density has somewhat larger amplitude giving a redder spectrum. At higher frequencies the simulation with noise and the observations indicate weaker periods near 24 months.

It should be noted that this shift in the dominant period is not observed in either the Blanke et al. (1997) hybrid coupled model or the Jin et al. (1996) intermediate coupled model. The reason for the shift in the model used here is not known. However, if a coupling strength parameter is introduced into the model without noise, the dominant period shifts to 48 months as the coupling strength increases. Perhaps, the noise forcing is, in effect, also modifying the coupling strength leading to a shorter dominant oscillation period.

3. Predictability experiments

The experiments presented in this section are designed to examine two aspects of ENSO predictability. First, it is shown how uncoupled atmospheric noise can lead to decadal variations in ENSO prediction skill. These decadal variations in forecast skill result without any changes to the climatological mean state of the model or any interactions between the Tropics and the extratropics. Second, it is shown that a simple delayed oscillator equation captures this same decadal variability. This result suggests that, during the predictable decades, the model is in a delayed oscillator regime, and in the unpredictable decades, the model is in a noise-driven regime.

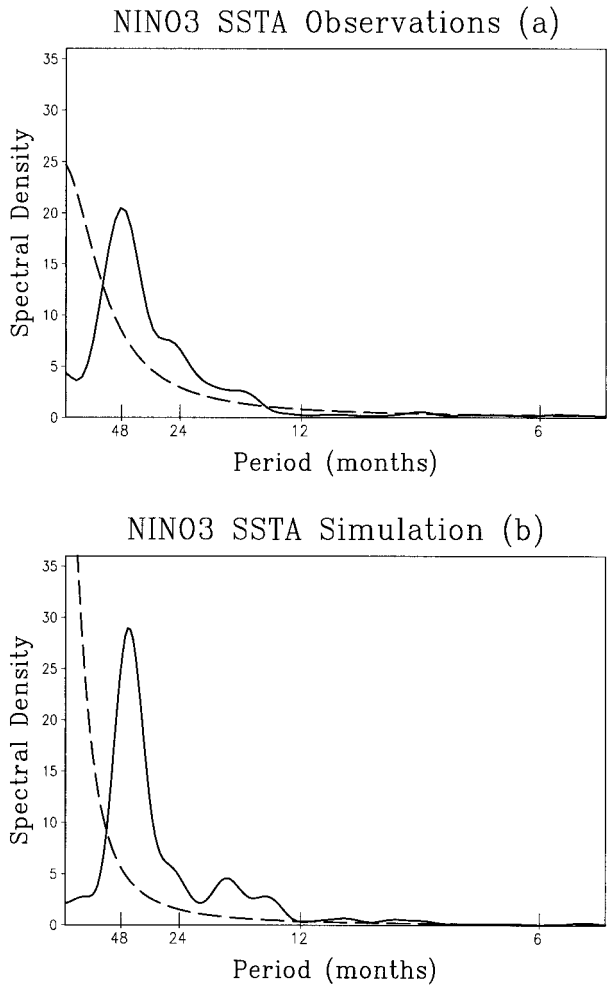

FIG. 4. Power spectra of (a) observed and (b) simulated NINO3 SSTA. The solid curve shows the power spectra, the dashed curve the power spectra for a red noise process.

a. Decadal variations in forecast skill and predictability

The long simulation with uncoupled atmospheric noise described in section 2 is used as initial conditions and to verify the prediction experiments. The predictions differ from the long simulation only in the uncoupled atmospheric noise, so that, at the initial time, the forecast and the verification are identical. During the evolution of the prediction experiments there is no external uncoupled noise forcing imposed. Predictions are made from each month of each year for years 101–200. The forecasts diverge from the verification because the noise is different and not because of sensitive dependence on the initial conditions.

Figures 5a,b show the 24-month evolution of the predicted and simulated SSTA in the NINO3 region for years 171–180 and 151–160, respectively. The evolution of each forecast is shown with the dashed curves and the verification is shown with the thick solid curve. These decades were chosen because the later decade (Fig. 5a) is characterized by higher-frequency, irregular and lower-amplitude variability; whereas the earlier (Fig. 5b) decade is dominated by regular larger-amplitude oscillations. Other than perhaps the warm period centered on year 179, the years 171–180 do not contain any significant warm or cold events. Most of this decade is dominated by temperatures that are slightly below normal. In contrast, the years 151–160 contain three well-defined warm and cold periods.

In general, the predictions initialized during years 171–180 do not produce erroneous warm or cold events, although there are some outliers. In agreement with the verification, most of the predictions give SSTA that is below normal; however, the forecasts fail to track the short-term variations in the simulation. Simulation years 151–160 are dominated by relatively large warm and cold events and the forecasts capture much of this variability. Superimposed on the low-frequency signal are short-term variations that the predictions fail to capture.

In ENSO forecasting, the standard technique for measuring prediction skill is to compute the correlation between predicted and observed NINO3 SSTA as well the root-mean-square error (rmse). Figures 6a–d show the NINO3 SSTA correlation coefficient and rmse for the same two decades shown in Figs. 5a,b. The simulation with noise is used as the ''observed'' in calculating the skill scores. The skill of the model is shown in the solid curve, and the skill of a persistence forecast is shown in the dotted curve. The correlation coefficient for the 1-month forecast (model or persistence) is the same for both decades; however, the correlation decays more rapidly for the predictions initialized during years 171–180. Using a correlation coefficient of 0.6 as a minimum measure of useful skill, during years 171–180 the model predictions are useful for lead times of up to 5 months; whereas, during years 151–160, the predictions are useful for lead times up to 12 months. Similarly, a persistence forecast is useful for about 3 months during years 171–180 and is useful for about 5 months during years 151–160.

In general, the rmse of the model predictions is consistent with the correlation coefficient. The rmse of the 1-month model forecasts are about the same for the two decades, but the rmse tends to increase more rapidly for the forecasts initialized during years 171–180. The rmse of the model predictions for years 171–180 and for years 151–160 exceed 0.8°C after 7 months and 11 months, respectively.[1] The model forecast rmse grows more rapidly and saturates earlier at a lower level during years 171–180 compared to years 151–160.

The rmse of the persistence forecasts have distinct characteristics that are worth noting. For example, the

[1] The value 0.8°C was chosen as a measure of maximum useful error because it corresponds to approximately two doublings of the 1-month forecast error.

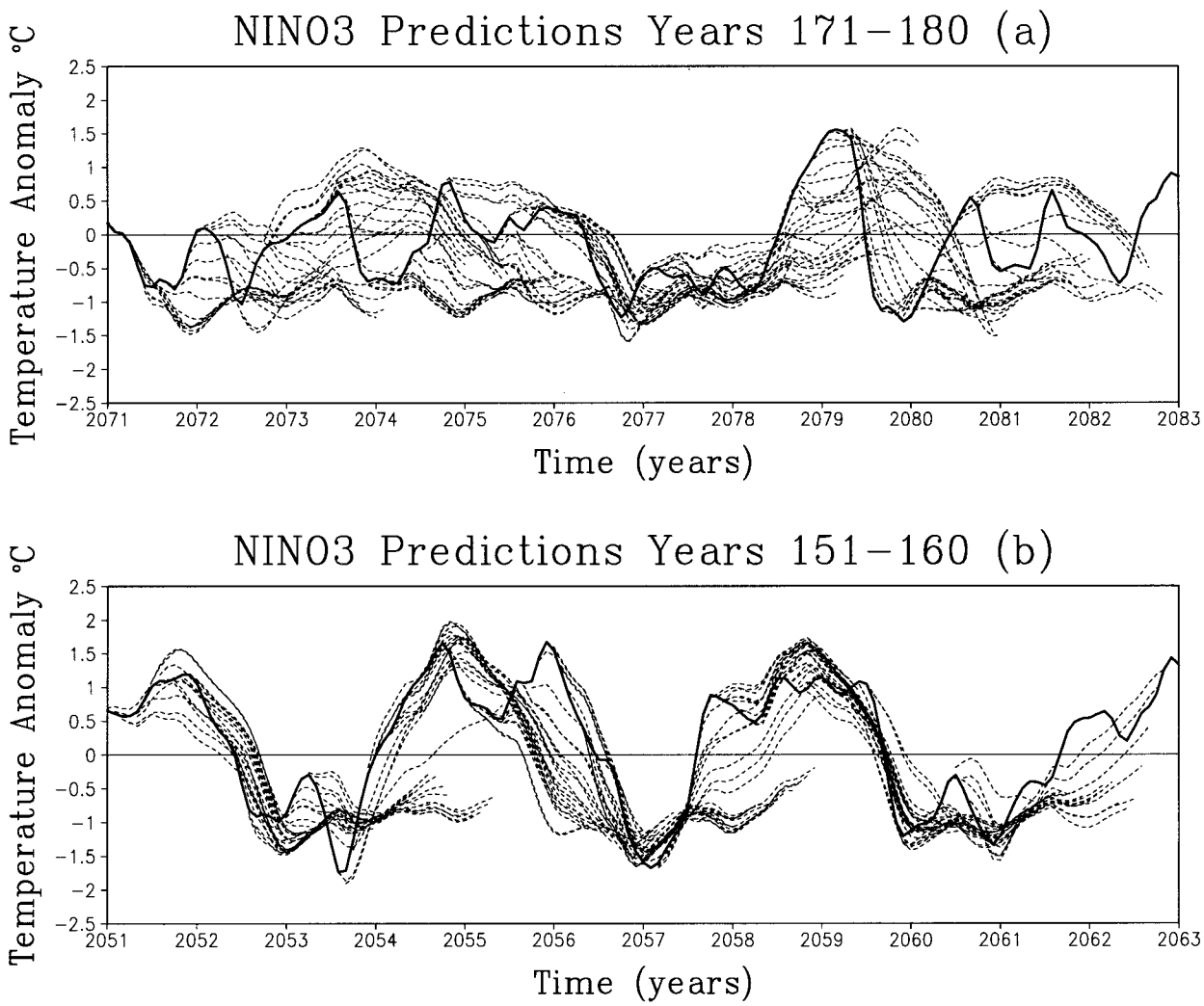

FIG. 5. Evolution of the NINO3 SSTA verification (solid line) and the prediction experiments (dotted lines) for the forecasts initialized during (a) years 171–180 and (b) years 151–160.

rmse of persistence is generally greater during years 151–160 than during years 171–180. In contrast to the correlation coefficient, the rmse of persistence indicates that a persistence forecast is more useful during years 171–180 than during years 151–160. The rmse of persistence grows more rapidly during years 151–160 and saturates at a considerably higher level. The higher level of rmse saturation for both the persistence forecasts and the model forecasts is consistent with the fact that the NINO3 SSTA variance is larger during years 151–160 than during years 171–180.

The decades between years 151–160 and 171–180 are representative of the entire time series. Figure 7a shows the NINO3 correlation coefficient evaluated over an 11-yr moving window for forecasts initialized each month of each year. The correlation coefficient plotted for year 120, for example, is calculated based on all forecasts initialized during years 115–125. There is a distinct decadal modulation of the correlation coefficient with some decades where the correlation remains above 0.6 for 15 months and some decades where the correlation drops below 0.6 after only 5 months. The decadal variability is not regular, but periods of high and low correlation persist for approximately 20 years.

The correlation coefficient and the rmse provide a measure of how well the forecasts predict the observations, and a significant degree of decadal variability has been found in these statistics. These statistics, however, cannot distinguish whether the decadal variations in skill are due to a fundamental property of the noise over the verification period or are inherent in the initial conditions. Given that the forecast experiments evolve without the uncoupled atmosphere noise forcing, a comparison of the forecasts independent of the observations (except as initial conditions) isolates the impact of the initial conditions in generating the decadal variations. The approach taken here is to examine the divergence of forecasts that are separated by 1 month and is similar

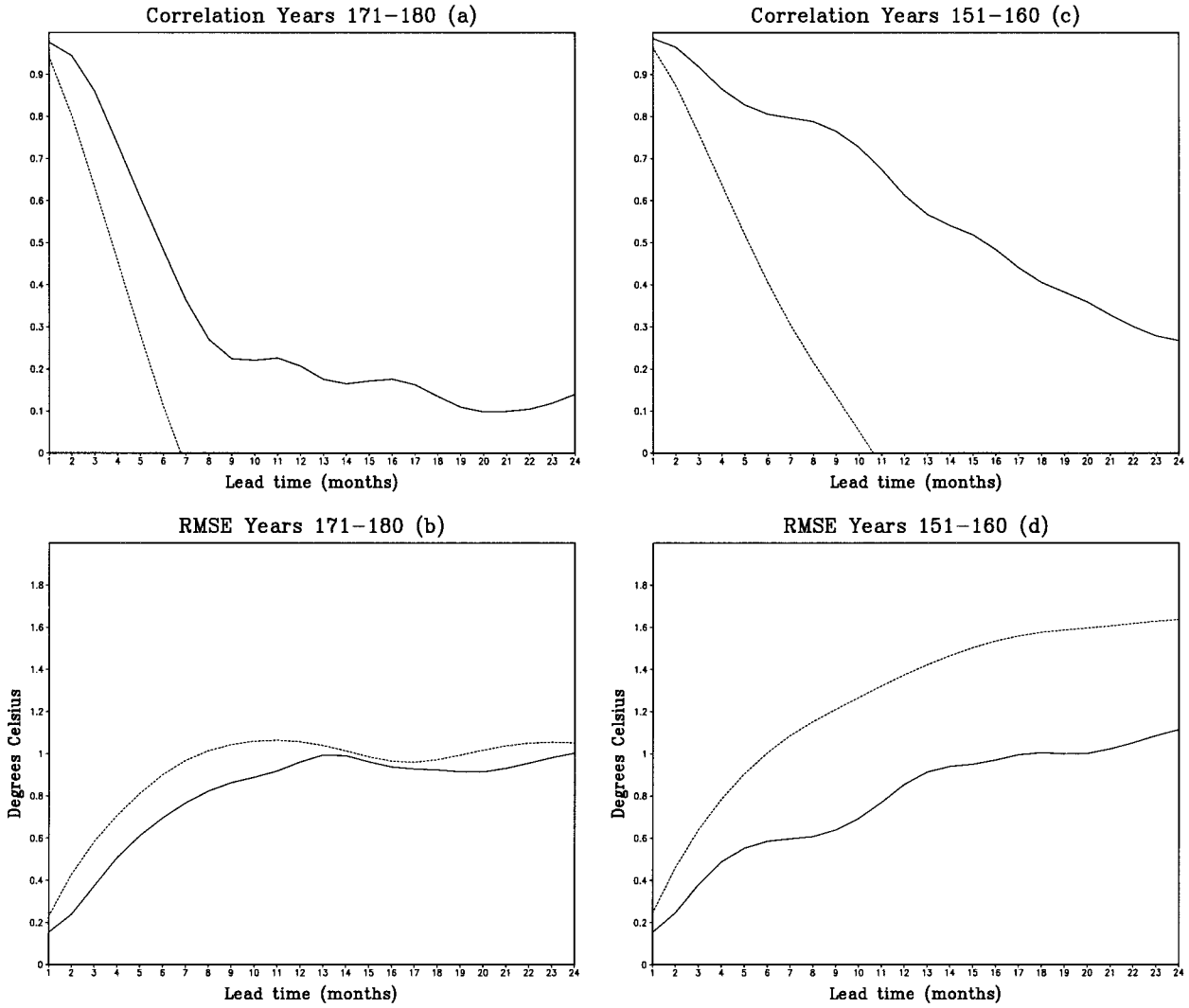

FIG. 6. Coupled model NINO3 SSTA correlation coefficient and rmse for (a), (b) years 171–180 and for (c), (d) years 151–160.

to the predictability calculations made by Goswami and Shukla (1991) and Shukla and Kirtman (1996).

Here we define the predictability as the time it takes small initial errors (where error is defined as the difference between consecutive forecasts valid at the same time) to saturate. For example, suppose $\psi_{i,j}$ is the predicted NINO3 SSTA corresponding to the jth month of the ith prediction. The mean error as a function of lead time ($k = 1, \ldots, 96$ months) where the initial error is equal to the 1-month prediction error is

$$E(k) = \left[\sum_{i=1}^{N-1} \frac{(\Psi_{i,k} - \Psi_{i+1,k-1})^2}{N-1}\right]^{1/2}. \quad (1)$$

In Eq. (1) N corresponds to the number of forecasts to be considered. We define E_{sat} as the average of $E(k)$ over lead times of 85–96 months. In the same format as Fig. 7a, Fig. 7b shows $E(k)/E_{\text{sat}}$ calculated over an 11-yr moving window ($N = 132$). The 11-yr running window was chosen because it removes much of the higher frequency variability while allowing the decadal signal to be seen. We have tried using both smaller and larger averaging periods with little qualitative difference. With this measure of predictability both the rate at which errors grow and their saturation value influence the predictability. In other words, it is possible for $E(k)$ to have large growth rates and large saturation values that may give the same predictability as small growth rates and small saturation values.

For short lead times (1–2 months) the error is generally 10%–30% of its saturation value. However, there are examples of 11-yr periods (years 257–267) where the error is at 90% of saturation by month 3. Typically, this rapid saturation is due to very low saturation values as opposed to large-error growth rates. Conversely, there are decades when the errors remain well below saturation for lead times greater than 18 months. For ex-

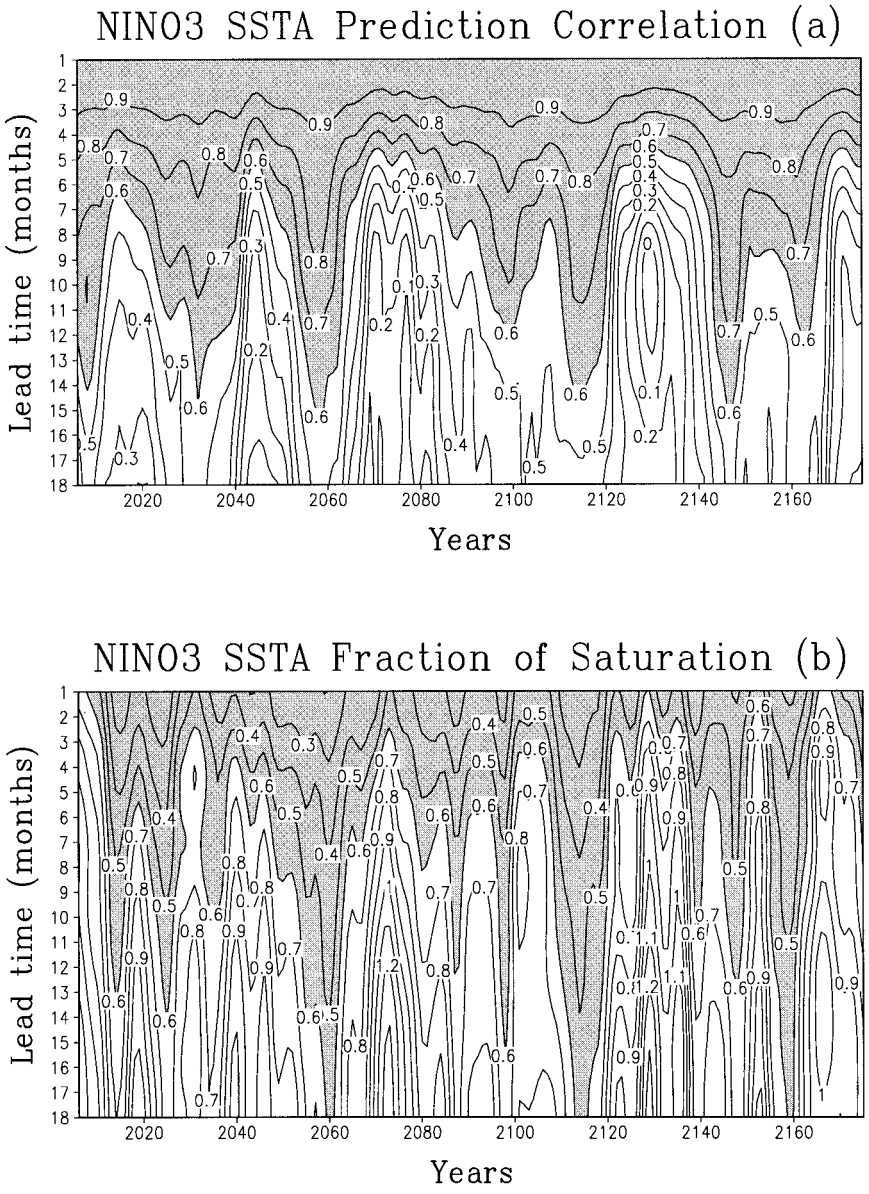

FIG. 7. NINO3 SSTA (a) correlation coefficient as function of lead time and (b) error of consecutive forecasts verifying on the same day as a function of lead time. The error is plotted as a fraction of the error saturation value. In both panels the calculation is made over an 11-yr moving window so that the values plotted for year 120 includes years 155–125. The contour interval is 0.1.

ample, during the 11-yr period centered on year 160, the error remains below 60% of saturation for all lead times up to 18 months. These periods of relatively large predictability are associated with both reduced error growth rates and larger saturation values. Supersaturation values are possible as the $E(k)$ fluctuates about its saturation value.

Comparison of Figs. 7a and 7b indicates that there is a large degree of consistency between the periods of high (low) correlation and high (low) predictability, although the correspondence is not perfect. For example, the predictability is quite low during the 11-yr period centered on simulation year 106, whereas the correlation is relatively high. Part of this discrepancy is due to the fact that the predictability measure has stronger higher-frequency signals than the 11-yr correlation coefficient. Using a somewhat broader window in calculating the correlation and the predictability measure improves the correspondence. Although not shown here, similar results were obtained in comparing the forecast rmse and the predictability.

In general, the prediction and predictability calcula-

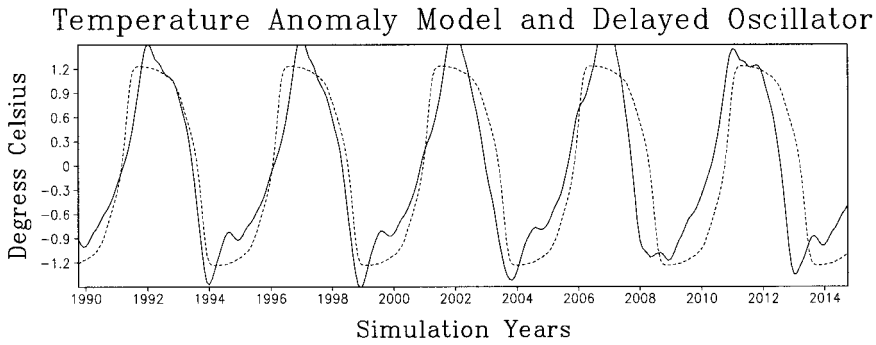

FIG. 8. Time series of NINO3 SSTA from the coupled model without noise (solid curve) and the delayed oscillator (dotted curve).

tions indicate that during decades when the interannual variance is relatively high, the forecast skill is relatively high and the limit of predictability is relatively long. Conversely, when the interannual variance is relatively low, the forecast skill is relatively low and the limit of predictability is relatively short.

b. The delayed oscillator

The forecast experiments described above suggest that, during decades when the model has strong regular oscillations, the prediction skill is high, and, during decades when the interannual variability is weak and irregular, the prediction skill is low. Given that this coupled model without uncoupled noise forcing is strongly driven by the delayed oscillator mechanism, we hypothesize that, during high-skill decades, the coupled model with noise is being driven by the delayed oscillator mechanism, and, when the skill is low, the delayed oscillator mechanism is not the dominant mechanism determining SSTA variability. In order to test this hypothesis, the delayed oscillator of Suarez and Schopf (1988) is used in similar prediction experiments.

The nondimensional delayed oscillator used here is described in detail in Suarez and Schopf (1988). Suppose T is a nondimensional temperature anomaly in the eastern Pacific. Then the evolution of T is described by

$$\frac{dT}{dt} = T - \alpha T(t - \delta) - T^3, \qquad (2)$$

where δ is the time delay and α gives the relative importance of remote wave effects versus local instability. For the prediction experiments presented here α and δ are chosen so that the delayed oscillator mimics the behavior of the coupled model without noise. We have not tuned α and δ for a best fit, but we have used values that give a reasonable fit to the coupled model. Figure 8 shows the NINO3 SSTA from the coupled model without noise and T by integrating Eq. (2) with $\alpha = 0.6$ and $\delta = 6.67$ (that corresponds to a 20-month delay). For the 24-yr period shown the two oscillations are largely in phase with similar amplitudes.

The delayed oscillator prediction experiments are made by initializing Eq. (2) with NINO3 SSTA from the control simulation of the coupled model with uncoupled atmospheric noise forcing. Figures 9a–d, to be compared with Fig. 6, show the skill scores for the delayed oscillator predictions for years 171–180 and years 151–160, respectively. During years 171–180, the skill of the delayed oscillator is almost indistinguishable from the skill of a persistence forecast, and during years 151–160, it beats persistence for all lead times in both the correlation and the rmse. The dependence of forecast skill on decade is the same as for the coupled model. In other words, when the coupled model forecast skill is relatively high (low), the delayed oscillator skill is also relatively high (low). Repeating the limit of predictability calculation with the delayed oscillator predictions also produces similar decadal variations.

While the decadal variations in forecast skill and predictability are similar, the actual values are lower with the delayed oscillator equation. This does not imply that the coupled model is in some sense a better forecast tool than the delayed oscillator equation. Additional tuning of α and δ would perhaps improve the delayed oscillator predictions, but this is beyond the scope of the current study. The success and failure of delayed oscillator predictions support the hypothesis that when ENSO is predictable and forecast skill is high, the delayed oscillator mechanism is controlling the variability and the noise has a minimal effect. Conversely, when the predictability is low and the forecast skill is low, the variability is dominated by the response to the noise forcing.

4. The decadal mean and ENSO variability

We have used a simple coupled model and an even simpler delayed oscillator equation to demonstrate that uncoupled atmospheric noise can lead to decadal variations in prediction skill and predictability. Moreover, we hypothesized that, during the predictable periods, the delayed oscillator mechanism describes the variability, and, during the unpredictable periods, the vari-

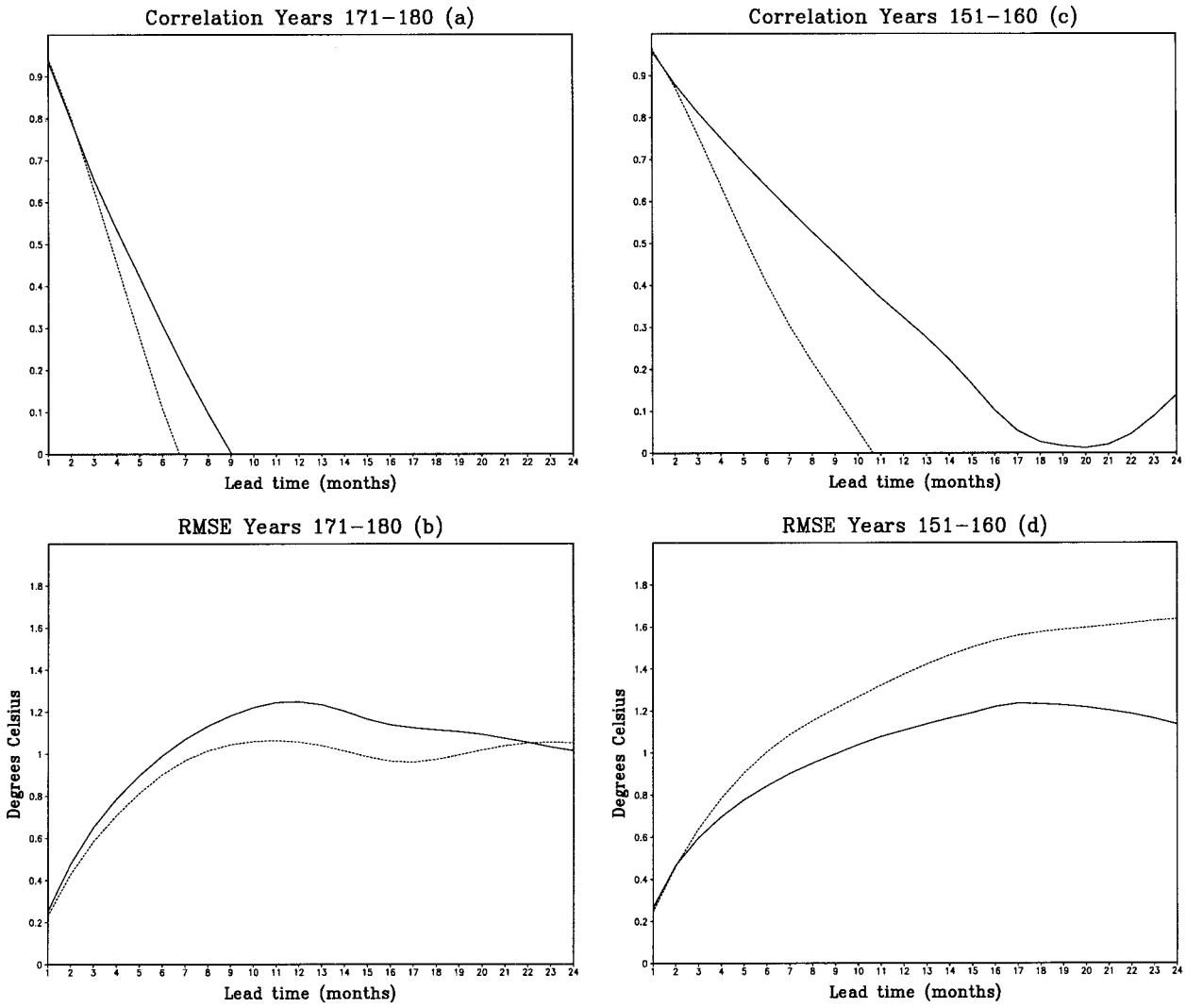

FIG. 9. Delayed oscillator NINO3 SSTA correlation coefficient and rmse for (a), (b) years 171–180 and for (c), (d) years 151–160.

ability is largely determined by the uncoupled noise forcing. The following experiments are intended to lend support to this hypothesis by demonstrating that slow timescale (decadal) changes in the state of the coupled model determine whether of the delayed oscillator mechanism or the external noise forcing is the dominant mechanism affecting the interannual SSTA variability.

Two sets of experiments are described here. In the first set of experiments, in addition to the internal variability in the coupled model, we prescribe a constant wind stress anomaly forcing. In these experiments, the prescribed wind stress anomaly is calculated from the predictable (years 151–160) and unpredictable (years 171–180) decades, respectively. The intent is to prescribe the mean state in the coupled model from either the predictable or unpredictable decade and examine how this affects the interannual variability of the SSTA. The second set of experiments demonstrate that the relative importance of the delayed oscillator versus the noise forcing in determining interannual SSTA variability is not an inherent property of the noise, but is determined by these slow timescale variations in the state of the coupled model.

a. Prescribed mean

We begin by showing the mean state of the coupled model from the predictable and unpredictable decades. Figures 10a–c show the 10-yr mean SSTA, wind stress anomaly, and thermocline anomaly from years 151–160 and Figs. 10d–f show the same fields for years 171–180. The predictable decade (years 151–160) is marked by warm SSTA, westerly wind stress anomalies, and consistent thermocline depth anomalies. Conversely, the unpredictable decade (years 171–180) is marked by mean easterlies, cold SSTA, thermocline shallowing in the east, and deepening in the west.

The simplest way to prescribe the two mean states

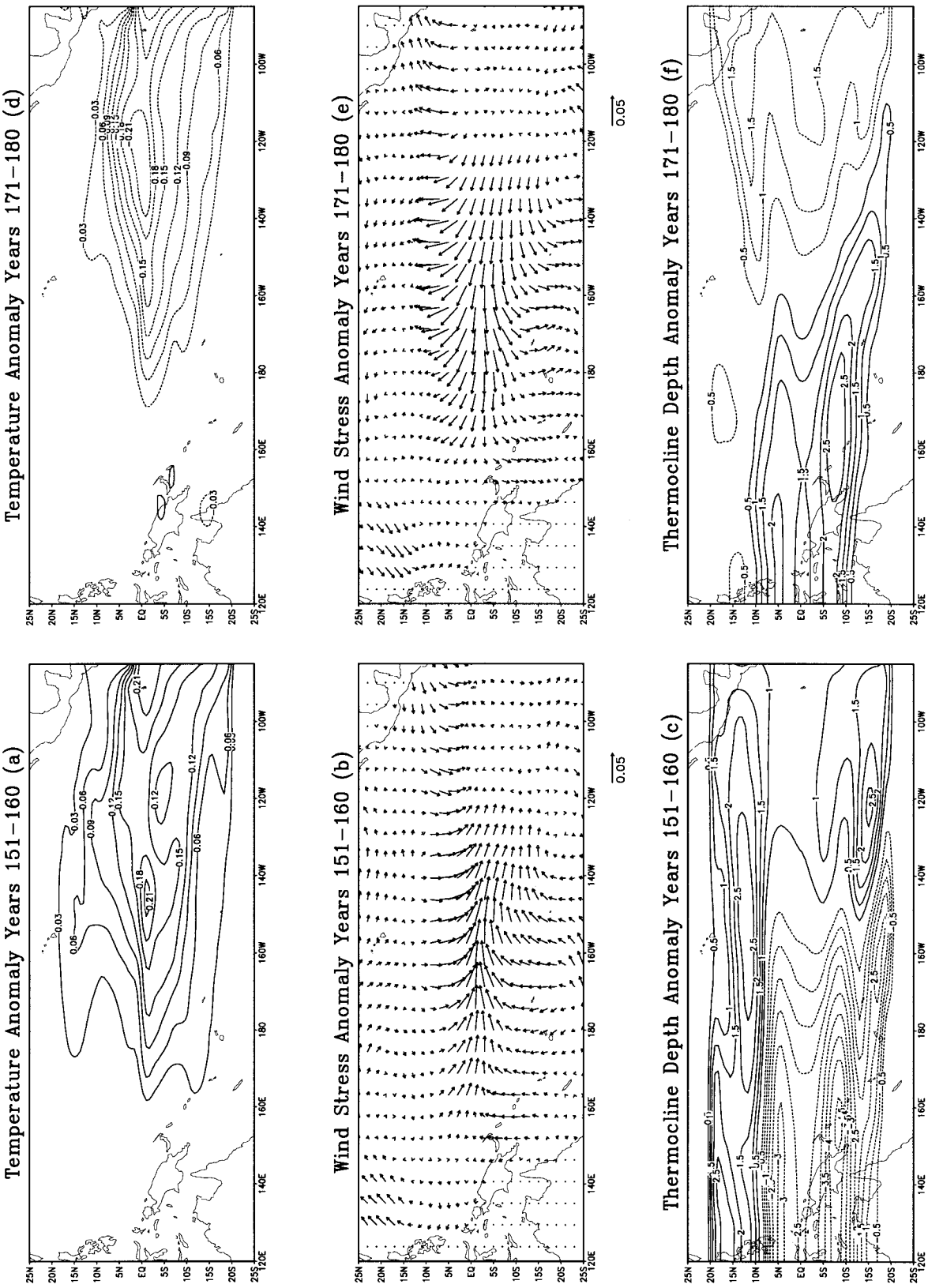

FIG. 10. Decadal mean SSTA, wind stress anomaly, and thermocline anomaly for (a)–(c) years 151–160 and for (d)–(f) years 171–180.

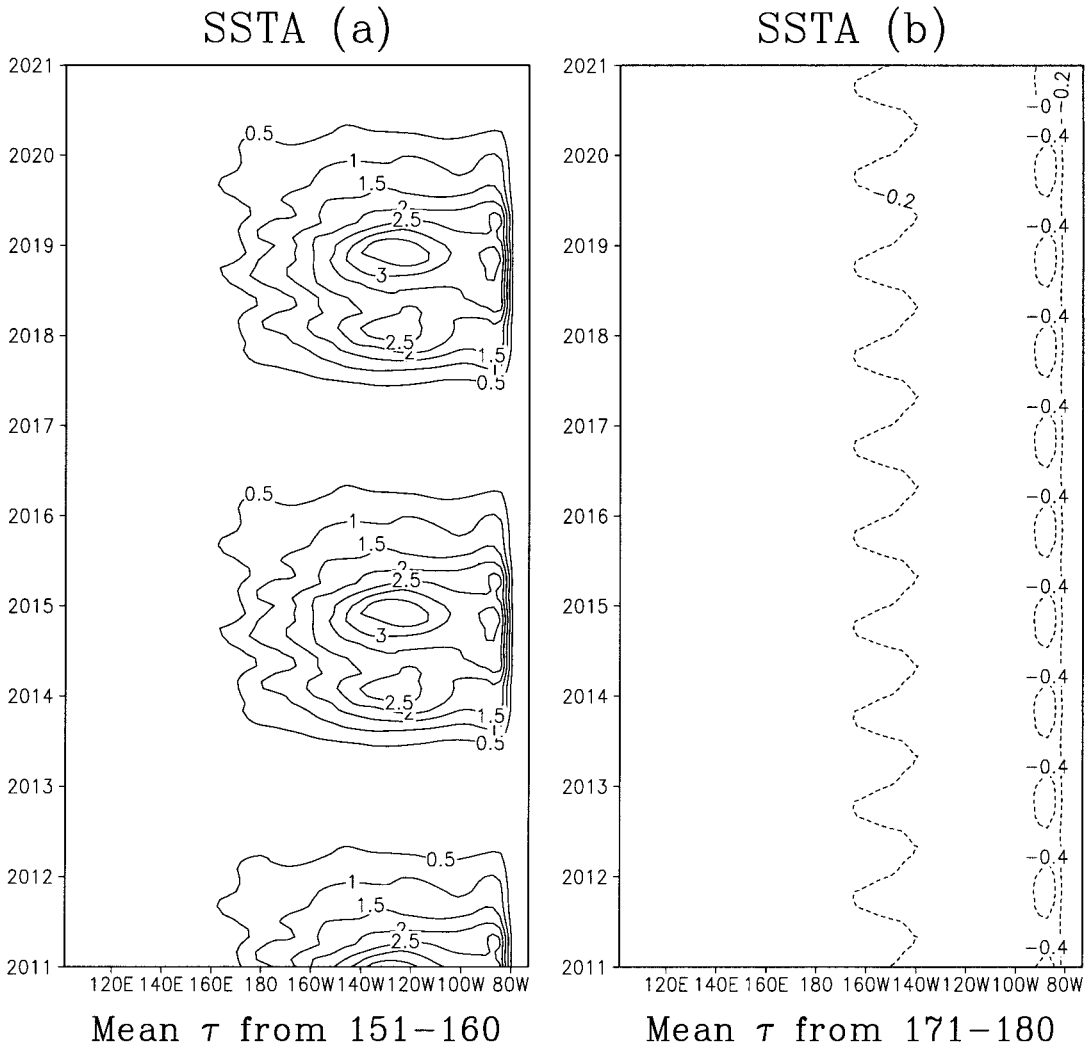

FIG. 11. Time–longitude cross section of the SSTA from a coupled model simulation without noise but with (a) prescribed mean westerlies from years 151–160 and (b) prescribed mean easterlies from years 171–180. In (a) the contour interval is 0.5°C and in (b) the contour interval is 0.2°C.

seen in Figs. 10a–f is to add a constant wind stress forcing to the coupled model. In two separate 100-yr simulations, the wind stress from Figs. 10b and 10e is added to the coupled model without noise forcing, respectively. Recall that without noise forcing the coupled model produces regular oscillations with a 5-yr period. Figures 11a,b show 10-yr time–longitude cross sections from these two simulations. When mean westerlies are prescribed (Fig. 11a) the model maintains strong interannual SSTA oscillations with a 5-yr period. The mean westerly bias is apparent. During the warm phase the SSTA exceeds 2.0°C for significant periods, but during the cold phase the SSTA remains above −0.5°C. In the simulation with prescribed mean easterlies (Fig. 11b), the cold bias is also readily apparent in that the SSTA is below zero throughout the basin. More remarkable, however, is that there is no interannual variations in the SSTA when mean wind stress anomaly from the unpredictable decade has been prescribed. In effect, without noise forcing the delayed oscillator mechanism has shut down.

We have repeated these two prescribed mean wind stress forcing simulations except in this case we have included the uncoupled noise forcing. Figures 12a,b show the slow timescale variability from the control simulation with and without noise and these two prescribed wind stress forcing simulations with noise, respectively. In Figs. 12a,b an 11-yr running mean of the NINO3 SSTA variance has been plotted. Again, the 11-yr averaging period was chosen for convenience. Modifying the averaging period has little qualitative impact on the results. In the control simulation with noise (Fig. 12a, solid curve) the decadal variations are readily apparent. During the predictable (unpredictable) decades the NINO3 SSTA variance is relatively large (small). For example, during years 151–160 (labeled 2051–

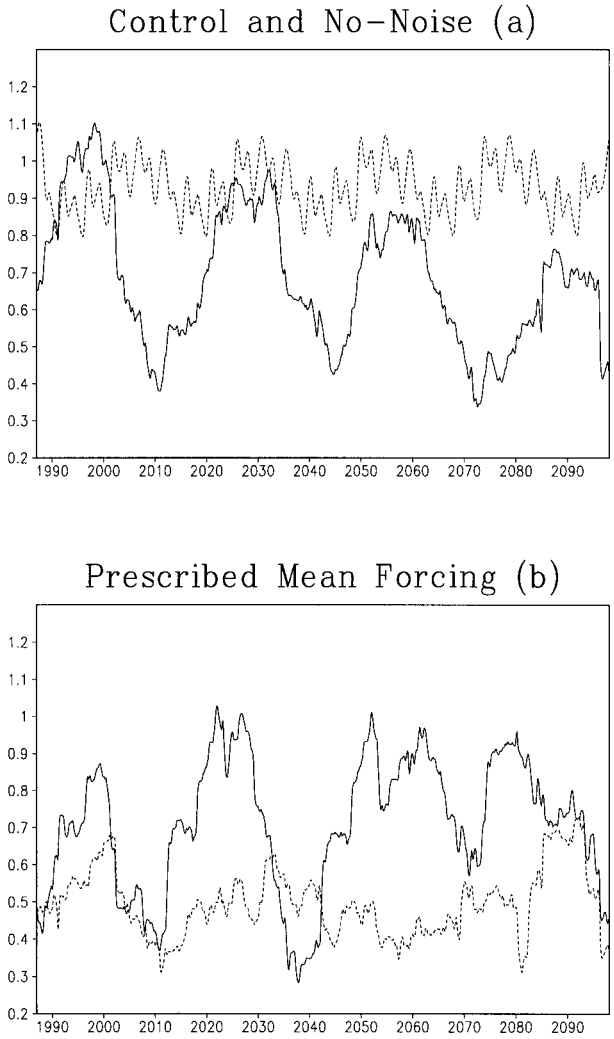

FIG. 12. NINO3 SSTA variance calculated over an 11-yr moving window for (a) the control coupled-model simulation with (solid curve) and without noise (dotted curve) and (b) the coupled model with noise and prescribed westerlies (solid curves) and prescribed easterlies (dotted curve).

2060) the NINO3 variance is generally slightly greater than 0.8 and during years 171–180 (labeled 2071–2080) the variance is generally below 0.4 and there are practically no ENSOs. The simulation without noise (Fig. 12a dotted curve) also has decadal-scale variations in the NINO3 variance, although these variations are considerably weaker than with the noise forcing. However, the model does not go through periods where there are no ENSO events. When the feedback from the external noise forcing is included, the decadal signal amplifies so that there are significant periods when the delayed oscillator mechanism is not dominating the SSTA variability.

Figure 12b shows what happens when uncoupled noise forcing is incorporated into the prescribed wind stress forcing simulations shown in Figs. 11a,b. In the case of prescribed mean westerly anomalies (solid curve), the character of the simulation is similar to the control simulation with decades of relatively high and low variance. There is some indication that the variance is somewhat larger with prescribed mean westerly anomalies than the control simulation with noise. With prescribed mean easterly anomalies (dotted curve), the NINO3 variance is considerably lower than either the control or the mean westerly anomaly simulations. When mean westerly anomalies are prescribed, the feedback from the noise forcing continues to produce decades where the variance is small and the variability is dominated by the noise and decades where the variance is large and controlled by the delayed oscillator mechanism. On the hand, when mean easterly anomalies are prescribed, the variability is greatly reduced and the noise forcing dominates the interannual SSTA variability.

b. Noise sensitivity

While the feedback from the uncoupled noise forcing is required to produce the large decadal variations in the coupled model simulations, the following two simulations indicate that these decade variations are due to changes in the mean as opposed to an inherent property of the noise. In order to demonstrate this point, two additional 10-yr integrations of the coupled model with noise were made. Simulation years 151–160 and 171–180 were repeated, but using different noise forcing. In repeating years 151–160, the uncoupled noise from years 171–180 was used and in repeating years 171–180, the noise from years 151–160 was used.

Figures 13a,b shows the NINO3 SSTA from these two additional simulations along with the control simulation. In both panels of Fig. 13, the solid curve gives the control simulation and the dotted curve corresponds to the experiments with the different noise forcing. Irrespective of the noise, years 151–160 are characterized by relatively strong ENSO oscillations, and years 171–180 are characterized by weak relatively high-frequency variability. In addition, prediction experiments using these two additional simulations as initial conditions give the same skill scores as the prediction experiments using the control simulation for initial conditions.

5. Summary

During the late 1980s and early 1990s, there was considerable success in forecasting tropical Pacific SSTA with coupled ocean–atmosphere models. More recently, the forecast models have had difficulty in predicting the SSTA. What has caused this change in prediction skill? At least four hypotheses arise: 1) interdecadal changes in the background state cause a change in regime that makes certain decades less predictable; 2) the character or details of external ''noise'' changes from decade to decade; 3) the observability of initial

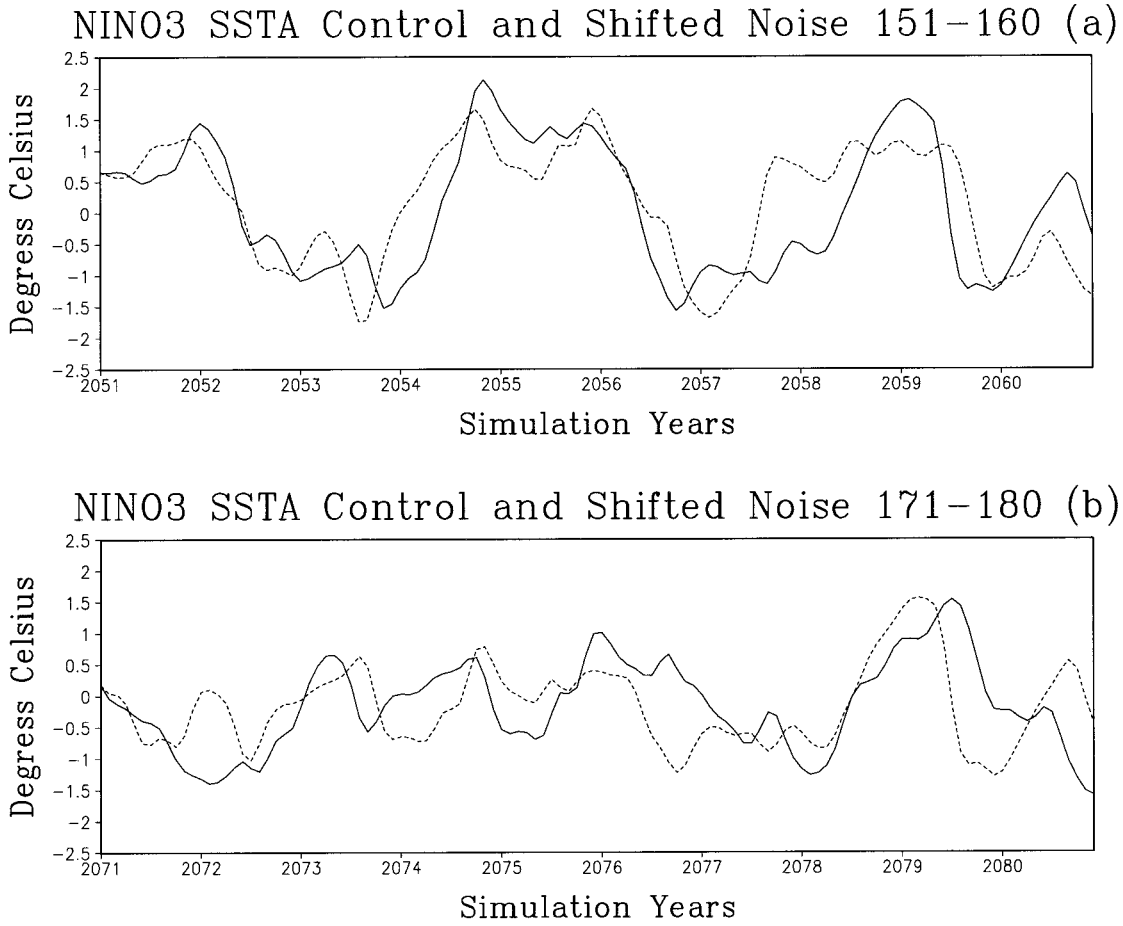

FIG. 13. Time series of NINO3 SSTA from the coupled model with noise. In (a) the control simulation from years 151–160 is shown with the solid line and the dotted line gives the simulation with the same initial condition as the control, but the noise is taken from the control simulation for years 171–180. In (b) the control simulation from years 171–180 is shown with the solid line and the dotted line gives the simulation with the same initial conditions as the control, but the noise is taken from the control simulation for years 151–160.

states changes from decade to decade, so the skill of initialization techniques varies; or 4) such measures as NINO3 correlation coefficient are unrepresentative and the results are not statistically significant.

Before abandoning hope and opting for the fourth explanation, we have undertaken a study to investigate the nature of changes in ENSO predictability. By conducting identical twin model experiments, we can make large enough ensembles to reduce the uncertainty of the measure, and we can completely eliminate the third alternative from our consideration by experimental design (although any real-world prediction system will remain confronted by initialization issues).

The results presented here are optimistic in terms of predicting ENSO. When the delayed oscillator mechanism is controlling the interannual SSTA variability, the prospects for useful ENSO predictions are good in spite of the fact that there is ample noise in the atmosphere serving to limit the predictability. Part of the reason that the predictable decades are so predictable is that the delayed oscillator mechanism is robust in terms of maintaining self-sustained oscillations during those decades. If the delayed oscillator does not maintain self-sustaining oscillations the limit of predictability is reduced becoming more like the unpredictable decades. Moreover, understanding the mechanisms for the contrasts in predictability may permit a priori prediction of whether the ENSO system is in the relatively predictable or unpredictable regime.

The contrasts between the 1980s and the early half of the 1990s have led to several investigations into the decadal variability of ENSO. Torrence and Webster (1996), for example, found that the amplitude of NINO3 SSTA during the 1920s and 1930s was approximately half of what it was during the 1970s and 1980s. It has been suggested that changes in the mean state are the source of decadal modulation of the interannual variability. In particular, Gu and Philander (1997) suggest that thermocline ventilation in the midlatitude oceans can be responsible for the changes in the mean state

that ultimately leads to the decadal variability. Whether such changes lead to changes in the predictability remains to be seen.

A question arose at the outset of this study as to whether changes in the mean state or changes in the uncoupled noise were responsible for interdecadal changes in predictability. Perhaps the years 171–180 were more irregular because the noise was of a different character, or interfered with the oscillator in a different way. By undertaking a set of experiments where the noise from the early decade was interchanged with the noise from the later decade, we were able to demonstrate that the difference in predictability was independent of the noise.

The prediction and predictability experiments presented here support the hypothesis that there are decadal changes in the mean state of the tropical Pacific that lead to decadal variability in ENSO. However, the mechanism for this variability does not require any anthropogenic climate change or interactions between the tropical and midlatitude oceans via thermocline subduction and ventilation. In the model presented here, the decadal signal is part of the basic ENSO oscillation without any atmospheric high-frequency variability. This decadal signal appears as a modulation of the amplitude of the interannual variability that is also associated with a relatively slow timescale modulation of the mean anomaly in the coupled model. Incorporating atmospheric high-frequency variability in the model enhances the amplitude of the decadal signal leading to decades when the ENSO variability is strong, much like the 1980s, and decades when the variability is weak and of higher frequency, much like the 1990s.

The coupled model used here is described in Kirtman (1997) and includes the Zebiak and Cane (1987) ocean model coupled to a very simple statistical atmosphere model. In extended integrations, this model produces regular ENSO oscillations with a 5-yr period. In addition to the 5-yr period, there is a weak amplitude modulation of the interannual variability with an approximate 20-yr period. We have incorporated the effect of high-frequency atmospheric variability on the ENSO oscillation by using observed wind stress data to define uncoupled atmospheric noise forcing that is then added to the atmospheric component of the coupled model. When the noise is included in the coupled model, irregular interannual variability results, and the dominant interannual period shifts to approximately 4 yr. The uncoupled noise also serves to amplify the decadal signal leading to extended periods when the variability is weak and of relatively high frequency and decades where the variability is strong and regular.

Using this long simulation (or control run) with noise for initial conditions and verification a large ensemble of prediction experiments was made. The prediction experiments differ from the control run in that there is no uncoupled noise forcing. In the prediction experiments, the initial condition was known exactly, but the high-frequency variability in the atmosphere was not simulated. By performing the prediction experiments in this way, we addressed how a poor simulation of atmospheric high-frequency variability can lead to decadal variations in ENSO predictability and prediction skill.

Using NINO3 SSTA correlation coefficient and rmse to verify the predictions indicates that there are decades when the forecasts are skillful for all lead times up to 15 months and there are decades when the skill falls off after only 5 months. The limit of predictability was also calculated based on how long it takes small initial errors in the predictions to saturate. This predictability measure varies decadally, similar to the skill scores. The predictable decades are characterized by relatively high forecast skill and relative large amplitude regular ENSO oscillations. On the other hand, the unpredictable decades are characterized by low forecast skill and relatively weak and relatively high-frequency variability.

During the predictable decades, the delayed oscillator mechanism is effective in determining the variability, and during the unpredictable decades, the delayed oscillator mechanism is ineffective, and the variability is determined by the uncoupled noise forcing. Prediction experiments using the delayed oscillator support this argument. We showed that the predictable decades are characterized by decadal mean westerly wind stress anomalies and warm SSTA. Moreover, when this mean state is prescribed in the coupled model only modest changes were noted in the interannual variability of the SSTA. On the other hand, the unpredictable decades are dominated by cold SSTA and easterly wind stress anomalies. Once these anomalies are prescribed, the delayed oscillator mechanism is damped and there are no ENSO oscillations. The interdecadal variability is an oscillation between two states: one where the delayed oscillator controls the variability and ENSO is highly predictable and the second state where the SSTA is primarily driven by the noise and is relatively unpredictable.

These results should be interpreted within the context of the model. There are a number of model deficiencies beyond the oversimplified statistical atmosphere. For instance, the ocean model includes only one baroclinic mode so that all the energy of the wind stress forcing must project onto this single mode; whereas in the real ocean, the wind stress forces a continuous spectrum of vertical modes. It is also possible that the decadal mode in the simulation without noise forcing is overemphasized due to simplifications in the model formulation.

It is an important point of these experiments that they are made with perfect initial conditions. The differences between the control run and the prediction lies entirely with the high-frequency ''uncoupled'' noise. Although the Zebiak–Cane model is expanded about an initial mean state, the model does not produce a zero-mean anomaly, and can undergo climate drift. If we define a background climatology to be the mean state of the Z–C system averaged over decades centered on the start of a run, then different experiments see different mean

states. But, because the models are initialized with perfect initial conditions, the effects of such changes in the mean state are perfectly assimilated into the prediction system. Changes in predictability are solely due to changes in the effect of uncoupled noise relative to the effects of the coupled oscillation.

It has been argued that the Z–C system failed to predict the 1990s because it was ''tuned'' or trained on the 1970–80s, and that if the model were retuned for the 1990s, improved predictions could be expected. Our results suggest that even with perfect initial tuning, certain decades will remain less predictable than others. The method of initializing from the full state of the control run causes all decadal changes in the basic state to be transferred to the prediction runs. It is solely the absence of random uncoupled noise that leads to prediction errors. Thus the results here show a limitation to the improvements in predictability that may be obtained through advanced data assimilation techniques or initialization strategies.

We should stress that our uncoupled noise is not the familiar weather variation, with an inherent predictability limit, but rather reflects all tropical variations that are not coupled to the ENSO oscillator. The low-predictive capability during certain decades may indeed be improved if better atmosphere–ocean models can demonstrate skill at simulating the noise. To directly demonstrate this point, we conducted a separate set of prediction experiments in which we simulated the ability to predict the noise. Recall that the original predictions were made by removing all noise but initializing from the exact state of the control run. To simulate the prediction of noise, we made the predictions with the noise added back in, but with an exponential decay of its amplitude. With no decay, the model reproduces the control run exactly, with immediate decay, the model reproduces the original prediction result. As may well be expected, increasing the ''skill'' of the noise prediction (by lengthening the *e*-folding period) leads to an improvement of the skill of the predictions, but the improvement is quite linear; that is, an *e*-folding time on the noise of 3 months leads to an increase of about 3 months in the time it takes for the anomaly correlation to fall below 0.5.

These experiments should be viewed as neither refuting nor supporting the basic ideas contained within the Gu and Philander (1997) hypothesis. These results can be viewed as an alternative hypothesis to Gu and Philander (1997). If interdecadal changes in the mean state can be induced by the mechanism they propose, then our results indicate that they should have significant impacts on the degree of predictability. We believe that the exact source of interdecadal changes in the mean state are probably of little relevance to the changes in predictability.

Our conclusion is that the basic predictive skill of the tropical coupled ocean–atmosphere system model comes from the long-period oscillatory dynamics associated with the delayed oscillator, that this oscillator has interdecadal variations that make it more or less susceptible to perturbations from external nose. Advancements in modeling and observations may well enable us to determine whether the present state is in a more or less predictable regime, but no amount of data assimilation or initialization will enhance its predictability during periods when the oscillations are weak and the noise is strong. Because the external noise is not directly associated with high-frequency weather, hope for extending predictability during such periods lies with enhancing prediction of such external noise.

Finally, we return to the motivation for this study that was to examine the contrast in predictive skill between the 1980s and the early 1990s. The coupled model results presented here suggest that mean SST during the unpredictable periods (early 1990s) tend to be colder than the mean SST during the more oscillatory periods (the 1980s). We have examined the difference in observed SST averaged from January 1980 through December 1989 minus the average SST from January 1990 through December 1996. The tropical Pacific basin as a whole is warmer during the early 1990s than during the 1980s, whereas the coupled model would indicate otherwise. However, in a broad region of the equatorial eastern Pacific, the SST is warmer during the 1980s and has a spatial pattern quite similar to Fig. 10a. Given this difference in the mean SST during the 1980s and early 1990s, we can neither rule out the mechanism presented here nor global warming as being responsible for the constrasts between the 1980s and early 1990s.

Acknowledgments. This work has benefited from discussions with D. Straus and J. Shukla. Comments from D. Battisti and an anonymous review were extremely helpful in improving this manuscript. This work was supported under NOAA Grants NA26-GP0149, NA46-GP0217, NA95-AANAG0274, and NSF Grant ATM-93021354.

REFERENCES

Balmaseda, M. A., M. K. Davey, and D. L. T. Anderson, 1995: Decadal and seasonal dependence of ENSO prediction skill. *J. Climate,* **8,** 2705–2715.

Barnett, T. P., M. Latif, N. Graham, M. Flugel, S. Pazan, and W. White, 1993: ENSO and ENSO-related predictability. Part I: Prediction of equatorial Pacific sea surface temperature with a hybrid coupled ocean–atmosphere model. *J. Climate,* **6,** 1545–1556.

Battisti, D. S., 1988: Dynamics and thermodynamics of a warming event in a coupled tropical atmosphere–ocean model. *J. Atmos. Sci.,* **45,** 2889–2919.

——, 1989: On the role of off-equatorial oceanic Rossby waves during ENSO. *J. Phys. Oceanogr.,* **19,** 551–559.

——, and A. C. Hirst, 1989: Interannual variability in a tropical atmosphere–ocean model: Influence of the basic state, ocean geometry, and nonlinearity. *J. Atmos. Sci.,* **46,** 1687–1712.

Blanke, B., J. D. Neelin, and D. Gutzler, 1997: Estimating the effect of stochastic wind stress forcing on ENSO irregularity. *J. Climate,* **10,** 1473–1486.

Chang, P., B. Wang, T. Li, and L. Ji, 1994: Interactions between the seasonal cycle and the Southern Oscillation-frequency entrainment and chaos in an intermediate coupled ocean–atmosphere model. *Geophys. Res. Lett.,* **21,** 2817–2820.

——, L. Ji, B. Wang, and T. Li, 1995: Interactions between the seasonal cycle and El Niño–Southern Oscillation in an intermediate coupled ocean–atmosphere model. *J. Atmos. Sci.,* **52,** 2353–2372.

Chen, D., S. E. Zebiak, A. J. Busalacchi, and M. A. Cane, 1995: An improved procedure for El Niño forecasting. *Science,* **269,** 1699–1702.

Eckert, C., and M. Latif, 1997: Predictability of a stochastically forced hybrid coupled model of El Niño. *J. Climate,* **10,** 1488–1504.

Goldenberg, S. B., and J. J. O'Brien, 1981: Time and space variability of the tropical Pacific wind stress. *Mon. Wea. Rev.,* **109,** 1190–1207.

Goswami, B. N., and J. Shukla, 1991: Predictability of a coupled ocean–atmosphere model. *J. Climate,* **4,** 1–22.

Gu, D., and S. G. H. Philander, 1997: Interdecadal climate fluctuation that depend on exchanges between the Tropics and the extratropics. *Science,* **275,** 805–807.

Jenkins, G. M., and D. G. Watts, 1968: *Spectral Analysis and Its Applications.* Holden-Day, 525 pp.

Ji, M., A. Kumar, and A. Leetmaa, 1994: An experimental coupled forecast system, at the National Meteorological Center: Some early results. *Tellus,* **46A,** 398–418.

——, A. Leetmaa, and V. E. Kousky, 1996: Coupled model predictions of ENSO during the 1980s and the 1990s at the National Centers for Environmental Prediction. *J. Climate,* **9,** 3105–3120.

Jin, F.-F., J. D. Neelin, and M. Ghil, 1994: El Niño on the devil's staircase: Annual subharmonic steps to chaos. *Science,* **264,** 70–72.

——, ——, and ——, 1996: El Niño/Southern Oscillation and the annual cycle: Subharmonic frequency-locking and aperiodicity. *Physica D,* **98,** 442–465.

Kirtman, B. P., 1997: Oceanic Rossby wave dynamics and the ENSO period in a coupled model. *J. Climate,* **10,** 1690–1704.

——, and S. E. Zebiak, 1997: ENSO simulation and prediction with a hybrid coupled model. *Mon. Wea. Rev.,* **125,** 2620–2641.

——, J. Shukla, B. Huang, Z. Zhu, and E. K. Schneider, 1997: Multiseasonal prediction with a coupled tropical ocean global atmosphere system. *Mon. Wea. Rev.,* **125,** 789–808.

Kleeman, R., 1993: On the dependence of hindcast skill on ocean thermodynamics in a coupled ocean–atmosphere model. *J. Climate,* **6,** 2012–2033.

——, and S. B. Power, 1994: Limits to predictability in a coupled ocean–atmosphere model due to atmospheric noise. *Tellus,* **46A,** 529–540.

——, and A. M. Moore, 1997: A theory for the limitation of ENSO predictability due to stochastic atmospheric transients. *J. Atmos. Sci.,* **54,** 753–767.

Latif, M., D. Anderson, T. P. Barnett, M. A. Cane, R. Kleeman, A. Leetmaa, J. J. O'Brien, A. Rostati, and E. K. Schneider, 1998: TOGA review paper ''Predictability and Prediction.'' *J. Geophys. Res.,* **103,** 14 375–14 394.

Mantua, N. J., and D. S. Battisti, 1995: Aperiodic variability in the Zebiak–Cane coupled ocean–atmosphere model: Air–sea interactions in the western equatorial Pacific. *J. Climate,* **8,** 2897–2927.

Munnich, M., M. A., Cane, and S. E. Zebiak, 1991: A study of self-excited oscillations in a tropical ocean–atmosphere system. Part II: Nonlinear cases. *J. Atmos. Sci.,* **48,** 1238–1248.

Neelin, J. D, D. S. Battisti, A. C. Hirst, F.-F. Jin, Y. Wakata, T. Yamagata, and S. E. Zebiak, 1998: ENSO theory. *J. Geophys. Res.,* **103,** 14 261–14 290.

Shukla, J., and B. Kirtman, 1996: Predictability and error growth in a coupled ocean–atmosphere model. COLA Tech. Rep. 24, 11 pp. [Available from COLA, 4041 Powder Mill Rd., Suite 302, Calverton, MD 20705.]

Suarez, M. J., and P. S. Schopf, 1988: A delayed action oscillator for ENSO. *J. Atmos. Sci.,* **45,** 3283–3287.

Torrence, C., and P. J. Webster, 1996: Inherent limits to interannual predictability. Preprints, *Eighth Conf. on Air–Sea Interactions and Conference on the Global Ocean–Atmosphere–Land System (GOALS),* Atlanta, Georgia, Amer. Meteor. Soc., 74–77.

Trenberth, K., and T. J. Hoar, 1997: El Niño and climate change. *Geophys. Res. Lett.,* **24,** 3057–3060.

Tziperman, E., L. Stone, M. A. Cane, and H. Jarosh, 1994: El Niño and chaos: Overlapping of resonances between the seasonal cycle and the Pacific ocean–atmosphere oscillator. *Science,* **264,** 72–74.

Wang, B., 1995: Interdecadal changes in El Niño onset in the last four decades. *J. Climate,* **8,** 267–285.

Zhang, Y., J. M. Wallace, and D. S. Battisti, 1997: ENSO-like interdecadal variability: 1900–93. *J. Climate,* **10,** 1004–1020.

Zebiak, S. E., 1989: On the 30–60-day oscillation and the prediction of El Niño. *J. Climate,* **2,** 1381–1387.

——, and M. A. Cane, 1987: A model of El Niño and the Southern Oscillation. *Mon. Wea. Rev.,* **115,** 2262–2278.